No. 1A-15 $PbZrO_3$, Lead zirconate

(M = 346.4)

1a Dielectric anomaly of $PbZrO_3$ associated with a phase transition was reported independently by Roberts and Smolenskii in 1950. Antiparallel ionic shifts on the (001) projection of crystal structure were found by Sawaguchi et al. in 1951. In the same year antiferroelectric double hysteresis loops were found by Shirane et al. $PbZrO_3$ is the first compound in which double hysteresis loops were observed. 50Rob, 50Smo 51Saw1, 51Shi

b

phase	II [a])	I [a])
state	A [c])	P [a])
crystal system	orthorhombic [b])	cubic [b])
space group	Pbam $-D_{2h}^{9}$ [d])	Pm3m $-O_{h}^{1}$
Θ [°C]	230 [a])	

[a])50Rob
[b])51Shi
[c])51Saw1
[d])82Fuj, 82Tan1

The space group of phase II was examined by several authors [d]) with the conclusion that Pbam$-D_{2h}^{9}$ is a more reasonable choice than Pba2$-C_{2v}^{8}$. [e])

[e])57Jon

A rhombohedral polar phase can be induced by an electric field in the phase II, causing the double hysteresis loop. [f])

[f])54Shi

Scott and Burns reported that a ferroelectric region appears in cooling as an intermediate phase between the phases I and II; the temperature width of the phase is related to deviation from the crystal stoichiometry. [g])

[g])72Sco

T_{melt} = 1570 °C (incongruent). 67Fus

Semi-transparent with red-brown color. 78Ujm

Color: Pale yellow. 72Sco

2a Crystal growth:

flux method; see 55Jon, 64Fus, 78Ujm, 89Woj

hydrothermal method; see 68Kuz, 69Tsu

3a Monoclinic cell parameters: $a_{mon} = c_{mon}$ = 4.1604(2) Å, b_{mon} = 4.1111(2) Å, β = 90°05'28(10)" at RT (in phase II). 74Sha

Orthorhombic cell parameters: $a = 2a_{mon} \cos(\beta/2)$ = 5.8883(3) Å, $b = 4a_{mon} \sin(\beta/2)$ = 11.7581(6) Å, $c = 2b_{mon}$ = 8.2222(4) Å. 79Fuj, 82Tan1

b Relation between the pseudocubic and orthorhombic cells: Fig. 1A-15-001.

Crystal structure: Z = 8 in phase II. The crystal is antipolar along the a-axis in phase II. 51Saw1, 57Jon

Schematic picture of Pb ion shift: Fig. 1A-15-001.

Fractional coordinate of atoms based on the space group Pba2$-C_{2v}^{8}$: Table 1A-15-001.

Fractional coordinate of atoms based on the space group Pbam$-D_{2h}^{9}$:
Table 1A-15-002, Table 1A-15-003; Fig.1A-15-002.
Projection of ZrO_6: Figs. 1A-15-003...1A-15-005.
Bond distances between Zr and O: Fig. 1A-15-006.

X-ray diffraction study of electric-field-induced orthorhombic phase: see 84Leo

4 Thermal expansion: Figs. 1A-15-007...1A-15-010.

	$\alpha_{a'} \approx -0.05 \cdot 10^{-5}\,K^{-1}$, $\alpha_{c'} \approx 2.80 \cdot 10^{-5}\,K^{-1}$ in phase II, $\alpha_{a'} \approx 1.10 \cdot 10^{-5}\,K^{-1}$ in phase I, where $\alpha_{a'}$ and $\alpha_{c'}$ are the linear thermal expansion coefficients along the pseudotetragonal a' and c' axes, respectively.	52Saw1
5a	Dielectric constant: Figs. 1A-15-011...1A-15-013; see also	89Rol1, 84Ujm
	Dielectric dispersion: Fig. 1A-15-014, Fig. 1A-15-015; see also	65Pet
	Effect of p on κ: Fig. 1A-15-016, Fig. 1A-15-017.	
	Phase diagram in regard to p: Fig. 1A-15-018.	
	Phase diagram in T–E plane: Fig. 1A-15-019; see also	76Fes1, 78Fes
	Effect of particle size on Θ: see	90Yam
	Effect of oxygen vacancies on κ and P_r: see	84Ujm
	Effect of X-ray irradiation on κ and $\tan\delta$: see	82Sin
	Effect of replacing ^{90}Zr by ^{94}Zr on capacitance: see	90Hid
b	Effect of E_{bias} on κ and Θ: Fig. 1A-15-020, Fig. 1A-15-021; see also	75Ujm
c	Spontaneous polarization: Fig. 1A-15-022.	
	Remanent polarization: Fig. 1A-15-023, Fig. 1A-15-024.	
	Critical field: Fig. 1A-15-025; see also	76Fes2
	Weak ferroelectricity was reported; see	95Dai
d	Pyroelectric effect: see	86Rol
	Electrocaloric effect: Fig. 1A-15-026.	
6a	Heat capacity: Fig. 1A-15-027, Fig. 1A-15-028.	
	For the transition Θ_{II-I} : ΔQ_m = 1840 J mol^{-1}, ΔS_m = 3.68 J K^{-1} mol^{-1}.	52Shi
b	Thermal conductivity: Fig. 1A-15-029, Fig. 1A-15-030.	
7b	Electrostriction: Fig. 1A-15-031; see also	84Rol
8	Elastic compliances: Fig. 1A-15-032.	
9a	Birefringence: Fig. 1A-15-033, Fig. 1A-15-034.	
	Infrared spectra: Fig. 1A-15-035; see also	89LiS
	Optical spectra in visible range: Fig. 1A-15-036, Fig. 1A-15-037.	
	Optical absorption edge: see	84Zam
10	Raman scattering: Fig. 1A-15-038, Fig. 1A-15-039; see also	89LiS
	For slightly Ti doped single crystal: Figs. 1A-15-040, 1A-15-041, 1A-15-042; see also	90Kug
	For pressure effect on the Raman spectra: see	94Men
11	Electrical conductivity: Fig. 1A-15-043, Fig. 1A-15-044; see also	76Pro, 74Ujm, 75Ujm
	Seebeck effect: Fig. 1A-15-045, Fig. 1A-15-046; see also	78Han
	At high temperature (340...600 °C), it is a p-type conductor.	72Ujm
	Photoconductivity: the maximum occurs at λ = 360 nm.	78Pro
	Drift mobility: see	80Pri
	Breakdown field: see	79Fes
12	Effect of magnetic field on dielectric properties: see	81Ism
13c	Mössbauer effect: Figs. 1A-15-047...1A-15-049.	

	Perturbed angular correlation: the temperature dependence of the electric field gradient on ^{181}Ta atom substituted for Zr atom.	74Ein, 75Tei, 75Sai
14a	Bragg reflection due to structural modulation: Fig. 1A-15-050.	
15	Antiferroelectric domain structure observed by etching method: see	69Gou
	Domain configuration in connection with atomic displacement studied by electron microscope: Fig. 1A-15-051.	
	Domain and twin structure observed by optical method: see	93Bal, 94Bah
	Zigzag-shaped domain boundaries: see	92Bal
16	Radiation damage: Fig. 1A-15-052.	
	Nonstoichiometry: see	80Pri
	Thermodynamical coefficients of the free energy are given in relating to the antiferro-electric-paraelectric transition.	74Mar

Table 1A-15-001. $PbZrO_3$. Atomic coordinates and shifts from ideal perovskite position at RT [57Jon]. The spacegroup is Pba2.

Atom	*x*	*y*	*z*	Wyckoff notation	Total shift [Å]
Pb'	0.706	0.127	0	4(c)	0.26
Pb''	0.706	0.127	0.500	4(c)	0.26
Zr'	0.243	0.124	0.250	4(c)	0.04
Zr''	0.243	0.124	0.250	4(c)	0.04
O(1)'	0.270	0.150	0.980	4(c)	0.35
O(1)''	0.270	0.100	0.480	4(c)	0.35
O(2)'	0.040	0.270	0.300	4(c)	0.53
O(2)''	0.040	0.270	0.750	4(c)	0.34
O(3)'	0	0.500	0.250	2(b)	0
O(3)''	0	0.500	0.800	2(b)	0.41
O(4)'	0	0	0.250	2(a)	0
O(4)''	0	0	0.800	2(a)	0.41

Table 1A-15-002. $PbZrO_3$. Structure of phase II [82Fuj]. Fractional coordinates of atoms refined by the combined X-ray and neutron diffraction profile analysis. (**a**): space group Pba2 where it is assumed that neither Pb or Zr have double periodicity along *c*-direction as proposed by Jona et al. [57Jon]. (**b**) and (**c**): two possible arrangements of atoms on the assumption that they are allowed to have double periodicity along the *c*-direction with the space group Pbam.

(a)	*x*	*y*	*z*	*B* [Å^2]
Pb	0.7064(2)	0.1266(2)	0.0	1.01(2)
Pb'	0.7064(2)	0.1266(2)	0.5	1.01(2)
Zr	0.2423(3)	0.125(1)	0.25	0.20(3)
O(1)	0.271(3)	0.156(2)	0.0	0.61(3)
O(1)'	0.288(3)	0.096(2)	0.5	0.61(3)
O(2)	0.032(2)	0.2608(6)	0.283(2)	0.61(3)
O(3)	0.0	0.5	0.206(2)	0.61(3)
O(4)	0.0	0.0	0.248(2)	0.61(3)
		R_{wp}(X) = 13.7 %		
		R_{wp}(N) = 7.7 %		

(b)	*x*	*y*	*z*	*B* [Å^2]
Pb	0.7064(2)	0.1247(3)	0.0	1.01(2)
Pb'	0.7064(2)	0.1285(3)	0.5	1.01(2)
Zr	0.2423(3)	0.125(1)	0.2581(5)	0.06(3)
O(1)	0.271(3)	0.156(2)	0.0	0.63(3)
O(1)'	0.287(3)	0.096(2)	0.5	0.63(3)
O(2)	0.032(2)	0.2616(7)	0.281(2)	0.63(3)
O(3)	0.0	0.5	0.205(2)	0.63(3)
O(4)	0.0	0.0	0.245(2)	0.63(3)
		R_{wp}(X) = 13.5 %		
		R_{wp}(N) = 7.9 %		

(c)	*x*	*y*	*z*	*B* [Å^2]
Pb	0.7064(2)	0.1247(3)	0.0	1.01(2)
Pb'	0.7064(2)	0.1285(3)	0.5	1.01(2)
Zr	0.2423(3)	0.125(1)	0.2416(5)	0.06(3)
O(1)	0.269(2)	0.155(2)	0.0	0.59(3)
O(1)'	0.291(3)	0.096(2)	0.5	0.59(3)
O(2)	0.032(2)	0.2610(6)	0.283(1)	0.59(3)
O(3)	0.0	0.5	0.206(2)	0.59(3)
O(4)	0.0	0.0	0.248(2)	0.59(3)
		R_{wp}(X) = 13.5 %		
		R_{wp}(N) = 7.5 %		

Table 1A-15-003. $PbZrO_3$. Structure of phase II [84Fuj]. Fractional coordinates of oxygen atoms determined by neutron profile analysis method, assuming (**a**) the space group Pbam and (**b**) additional modulation associated with Σ_3, R_{25}^{x} and R_{25}^{y} modes.

(a)	*x*	*y*	*z*
O(1)	0.2665(31)	0.1570(34)	0.0
O(1)'	0.2916(31)	0.0933(36)	0.5
O(2)	0.0295(19)	0.2590(9)	0.2809(20)
O(3)	0.0	0.5	0.2071(26)
O(4)	0.0	0.0	0.2520(27)
		R_{wp} = 6.6 %	

(b)	*x*	*y*	*z*
O(1)	0.2817(15)	0.1537(3)	0.0
O(1)'	0.2817(15)	0.0963(3)	0.5
O(2)	0.0352(19)	0.2593(10)	0.2791(3)
O(3)	0.0	0.5	0.2209(3)
O(4)	0.0	0.0	0.2209(3)
		R_{wp} = 7.5 %	

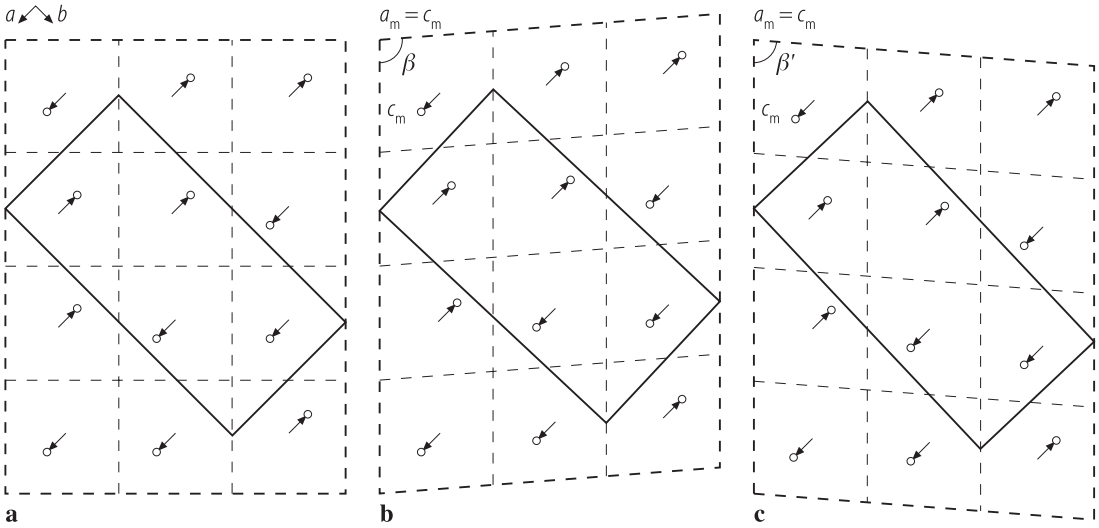

Fig. 1A-15-001. $PbZrO_3$. Schematic projection of $PbZrO_3$ cell on (001) in phase II. Arrows represent the direction of shifts of Pb ions. Dashed lines delineate the perovskite cell, and the solid lines show the orthorhombic cell. (**a**) Assumed tetragonal distortion of perovskite cell [51Saw1]. (**b**) Monoclinic distortion of perovskite cell [74Sha], $a = 2a_m \sin(\beta/2)$, $b = 4a_m \cos(\beta/2)$, $c = 2b_m$. (**c**) Reexamined monoclinic distortion of perovskite cell [79Fuj], $a = 2a_m \cos(\beta/2)$, $b = 4a_m \sin(\beta/2)$, $c = 2b_m$. The lattice slightly contracts along the direction of antiparallel shifts of Pb ions rather than the extension.

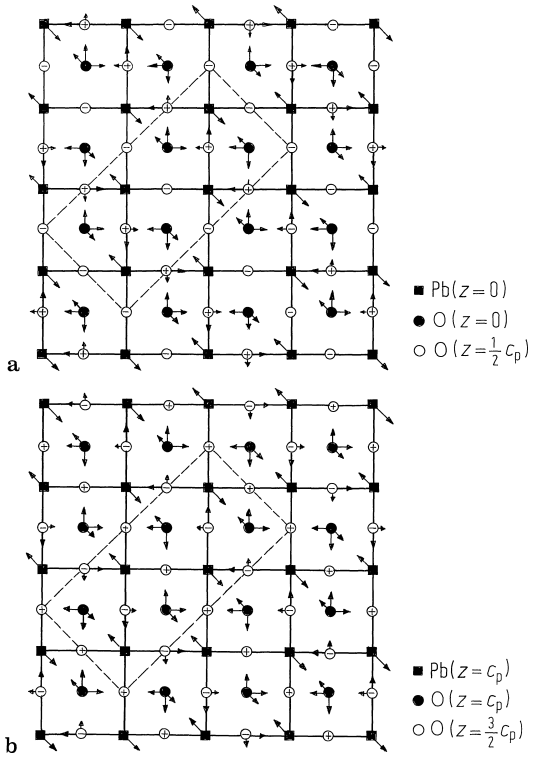

Fig. 1A-15-002. $PbZrO_3$. Structure of phase II [84Fuj]. Projection of atomic displacements associated with modes Σ_3, R_{25}^{x} and R_{25}^{y} on the *ab* plane. Determined by profile analysis of powder neutron diffraction. Zr atoms are not indicated because of their small shifts. Dashed line indicates the orthorhombic cell. c_p: pseudocubic lattice parameter in the *z* direction.

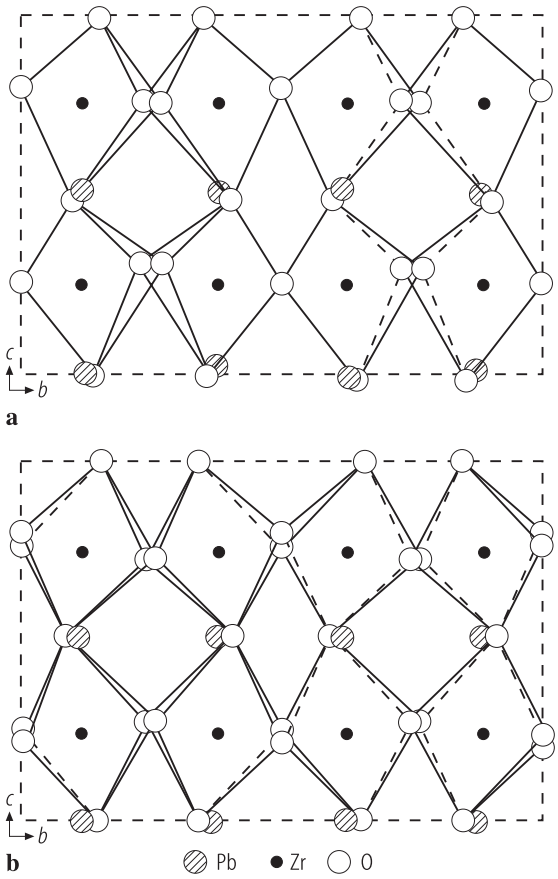

Fig. 1A-15-003. $PbZrO_3$. Schematic view of ZrO_6 octahedra network as seen along [100] direction. (**a**): structure given in [57Jon], (**b**): structure given in [82Fuj].

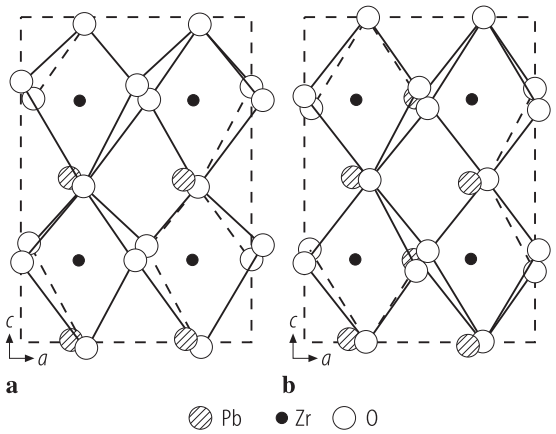

Fig. 1A-15-004. $PbZrO_3$. Schematic view of ZrO_6 octahedra network as seen along [010] direction. (**a**): structure given in [57Jon], (**b**): structure given in [82Fuj].

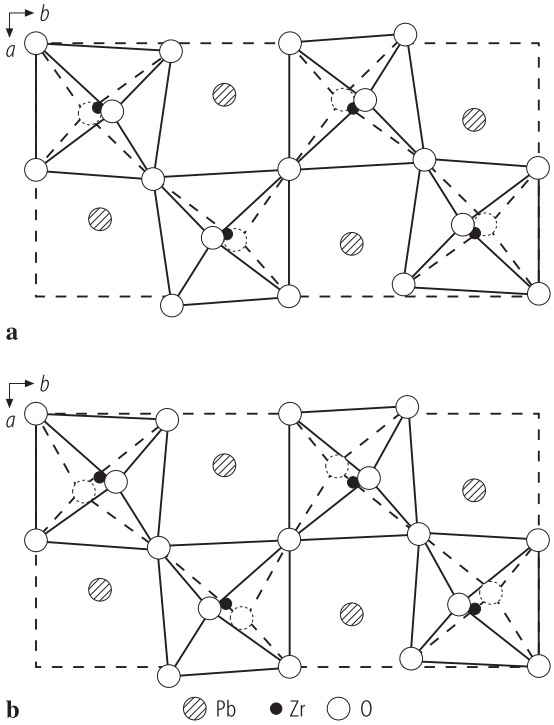

Fig. 1A-15-005. $PbZrO_3$. Schematic view of ZrO_6 octahedra network as seen along [001] direction. (**a**): structure given in [57Jon], (**b**): structure given in [82Fuj].

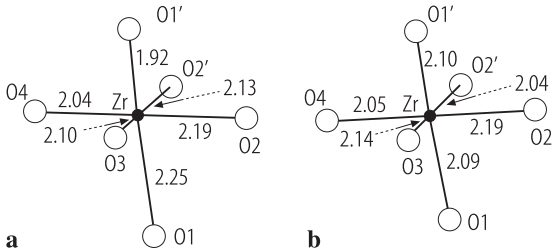

Fig. 1A-15-006. $PbZrO_3$. Comparison of environments of Zr involved in two structure analyses. Interatomic distances are given in Å. (**a**): structure given in [57Jon], (**b**): structure given in [82Fuj].

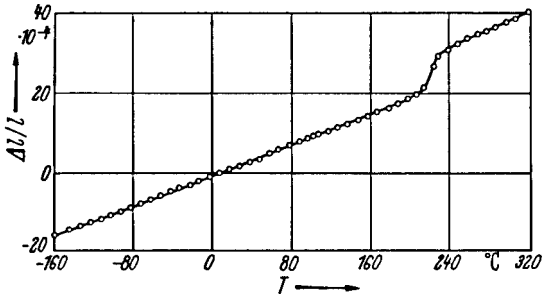

Fig. 1A-15-007. $PbZrO_3$ (ceramics). $\Delta l/l$ vs. T [50Shi].
$\Delta l/l$: linear thermal expansion.

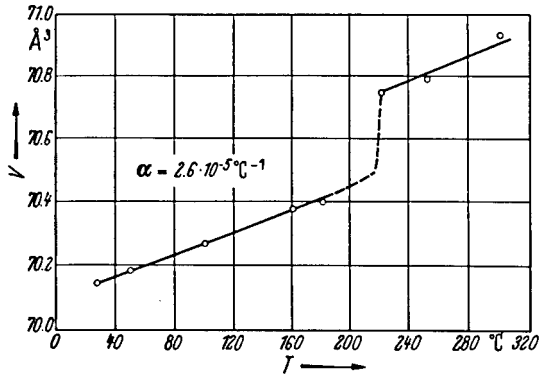

Fig. 1A-15-008. $PbZrO_3$ (ceramics). *V* vs. *T* [51Ued].
V : volume of the cubic or the pseudocubic unit cell.

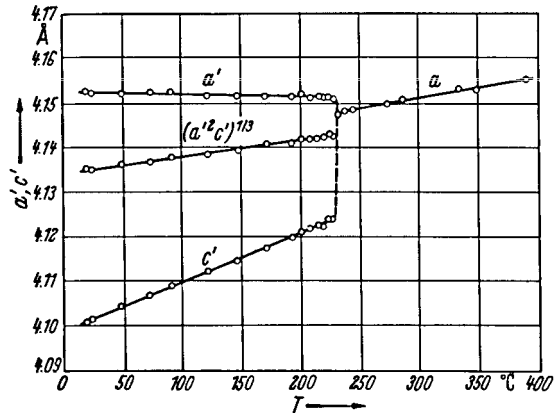

Fig. 1A-15-009. $PbZrO_3$ (ceramics). Unit cell parameters vs. T [52Saw1]. $a' \approx a_{mon} = c_{mon}$, $c' \approx b_{mon}$ (a pseudotetragonal unit cell was assumed).

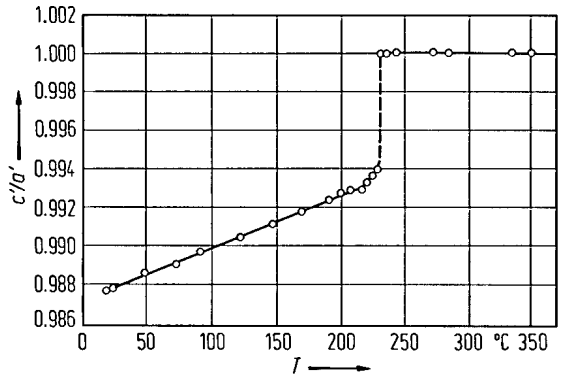

Fig. 1A-15-010. $PbZrO_3$ (ceramics). c'/a' vs. T [53Saw]. See the caption of the preceding figure for a' and c'.

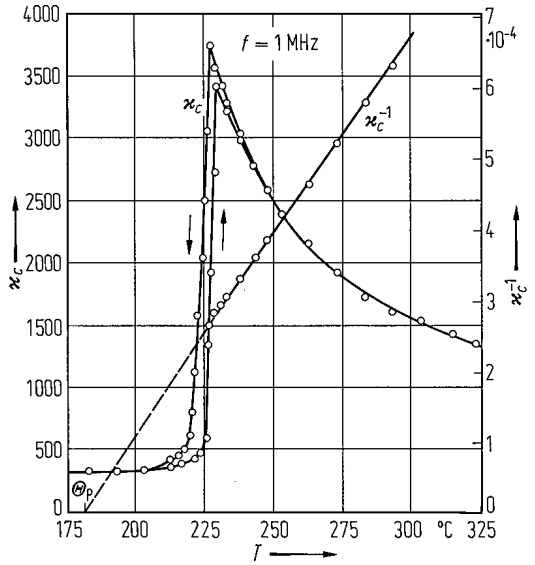

Fig. 1A-15-011. $PbZrO_3$ (single crystal). κ_c, κ_c^{-1} vs. T [78Ujm].

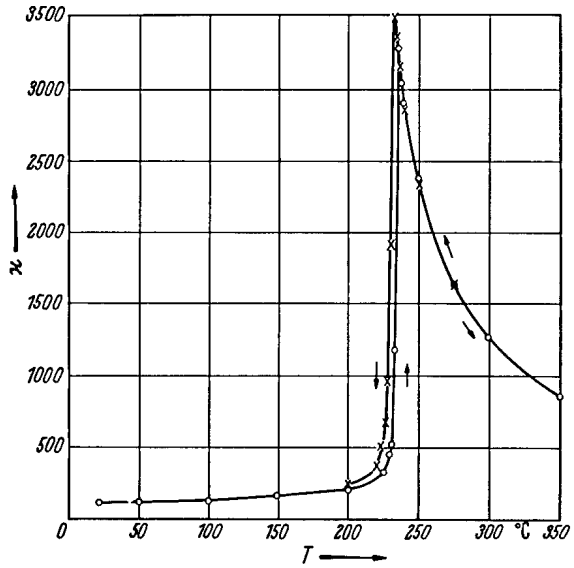

Fig. 1A-15-012. $PbZrO_3$ (ceramics). κ vs. T [50Rob]. f = 1 kHz.

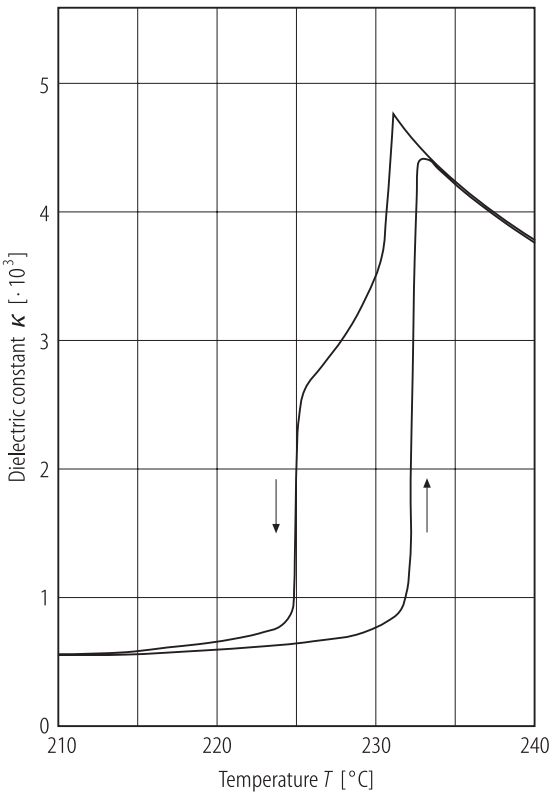

Fig. 1A-15-013. $PbZrO_3$ (ceramics with high concentration of defects). κ vs. T [88Ujm]. f = 150 kHz. The last sintering temperature was so high (1270 °C) that the ceramics contain an extremely high concentration of defects.

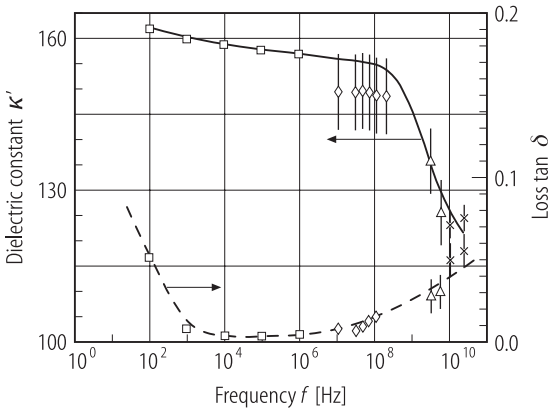

Fig. 1A-15-014. $PbZrO_3$ (ceramics). κ', $\tan\delta$ vs. f [88Lan]. Different marks correspond to different measurement methods. Squares: LCR bridge, diamonds: damped impedance, triangles: TM cavity, crosses: transmission.

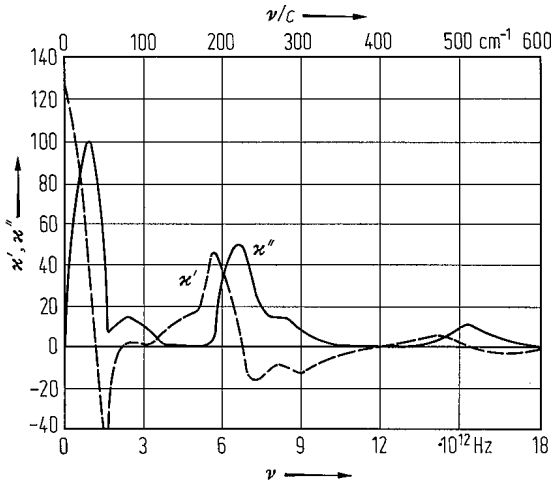

Fig. 1A-15-015. $PbZrO_3$. κ', κ'' vs. ν [65Per]. The curves are obtained from the reflectivity data using Kramers-Kronig relation.

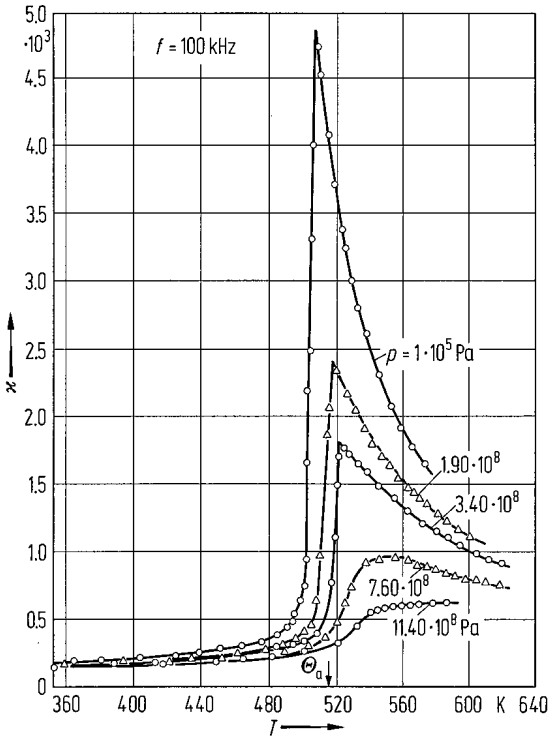

Fig. 1A-15-016. $PbZrO_3$ (ceramics). κ vs. T on heating [70Sam]. Parameter: p.

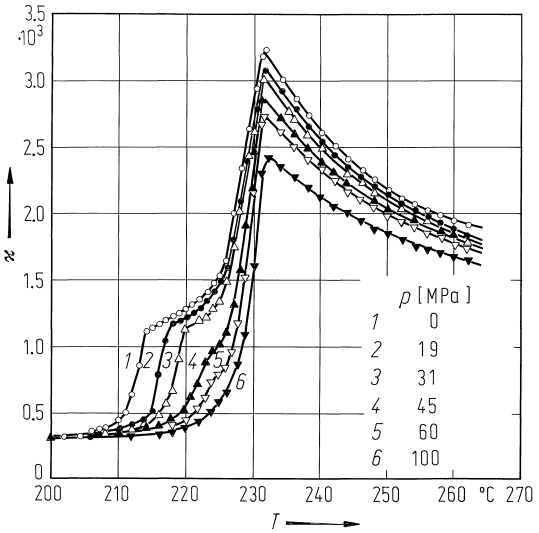

Fig. 1A-15-017. $PbZrO_3$ (ceramics). κ vs. T on cooling [85Ujm]. Parameter: p.

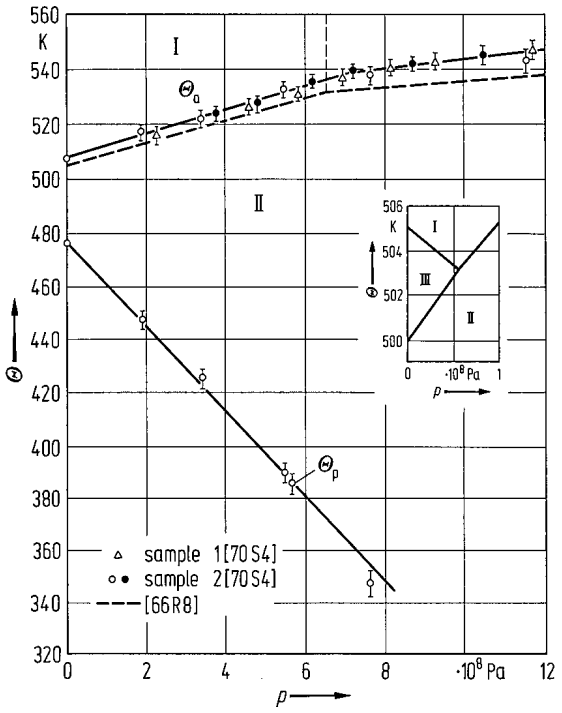

Fig. 1A-15-018. $PbZrO_3$. Θ vs. p [70Sam, 66Rap]. Phase III is an intermediate phase.

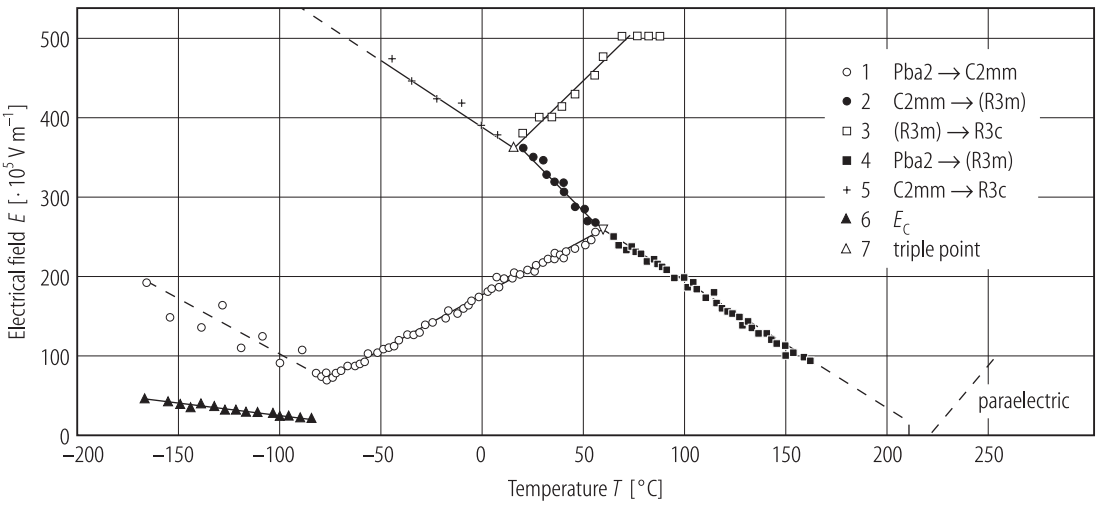

Fig. 1A-15-019. $PbZrO_3$. *E-T* phase diagram [79Fes]. *E*: electric field parallel to the *c*-axis of the phase II.

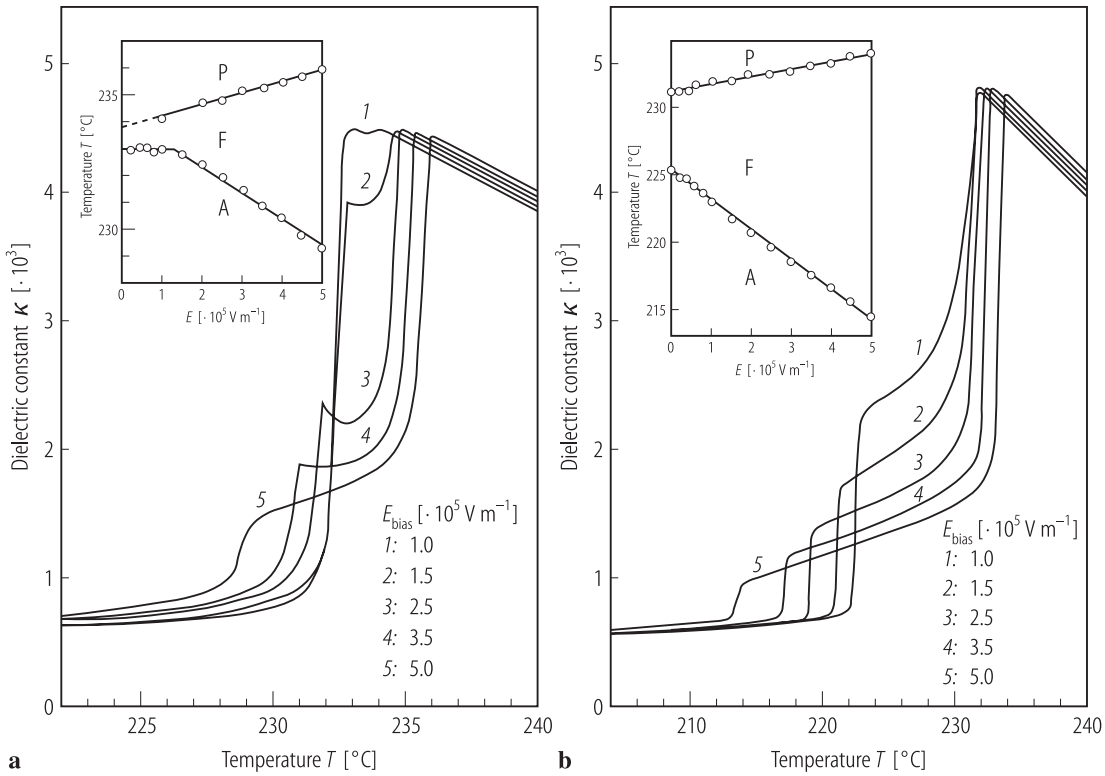

Fig. 1A-15-020. $PbZrO_3$ (ceramics with high concentration of defects). κ vs. T [88Ujm]. f = 150 kHz. Parameter: E_{bias}. (**a**): on heating, (**b**): on cooling. Inserts show E-T phase diagrams.

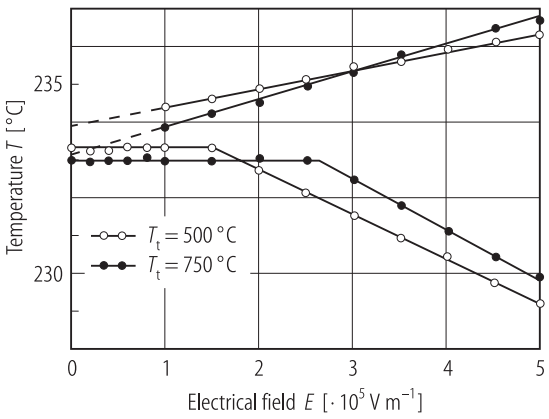

Fig. 1A-15-021. $PbZrO_3$ (ceramics with high concentration of defects). *E-T* phase diagram [88Ujm]. T_t : the temperature of heat-treatment in vacuum for 15 min.

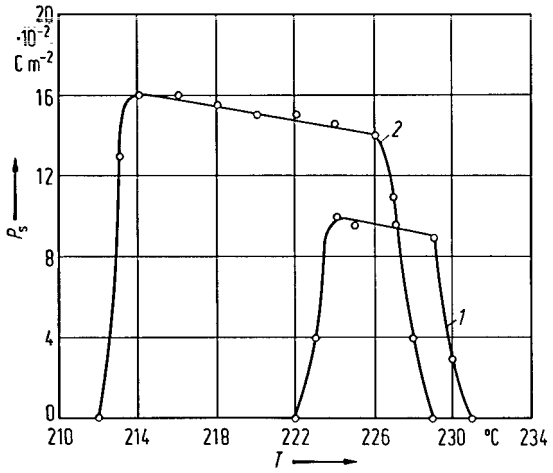

Fig. 1A-15-022. $PbZrO_3$ (single crystal). P_s vs. T [78Ujm].
Curve *1*: on heating, *2*: on cooling.

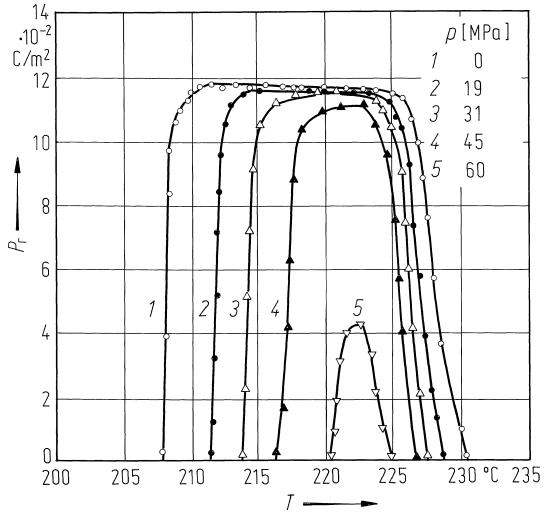

Fig. 1A-15-023. $PbZrO_3$ (ceramics). P_r vs. T [85Ujm]. P_r: remanent polarization. Parameter: p.

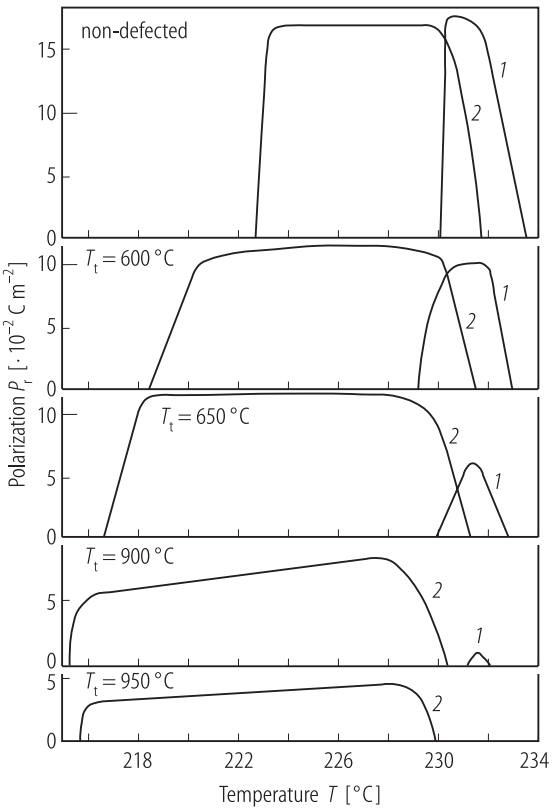

Fig. 1A-15-024. $PbZrO_3$ (ceramics with high concentration of defects). P_r vs. T [88Ujm]. T_t: the temperature of heat-treatment in vacuum for 15 min. Curve *1*: on heating, *2*: on cooling.

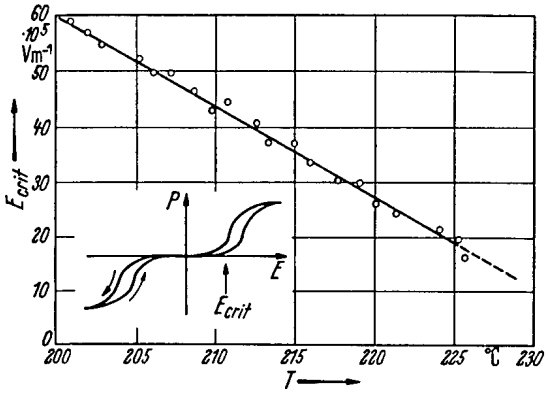

Fig. 1A-15-025. $PbZrO_3$. E_{crit} vs. T [52Saw2]. E_{crit}: critical field of antiferroelectric hysteresis loop.

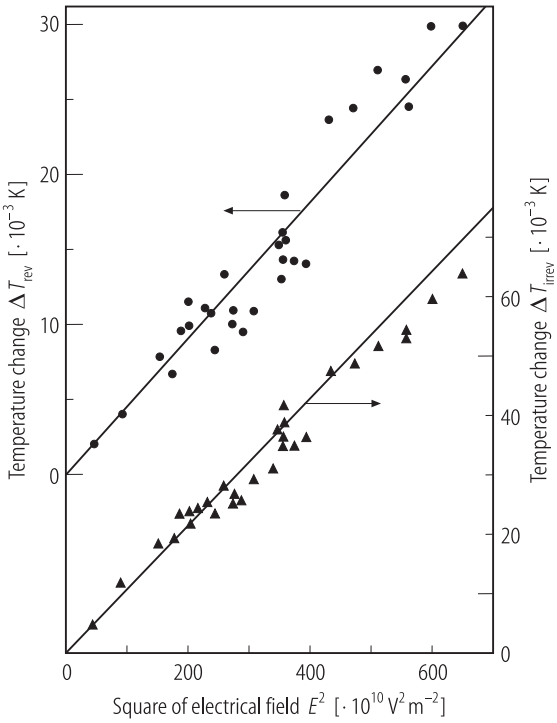

Fig. 1A-15-026. $PbZrO_3$ (ceramics). ΔT_{rev}, ΔT_{irrev} vs. E^2 [93Law]. ΔT_{rev}: reversible electrocaloric temperature change. ΔT_{irrev} : irreversible electrocaloric temperature change. E: applied electric field. T = 4.36 K.

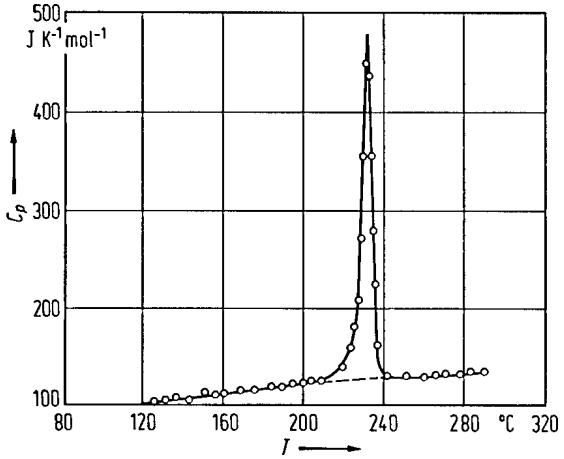

Fig. 1A-15-027. $PbZrO_3$ (ceramics). C_p vs. T [51Saw2].
C_p: molar heat capacity at constant pressure.

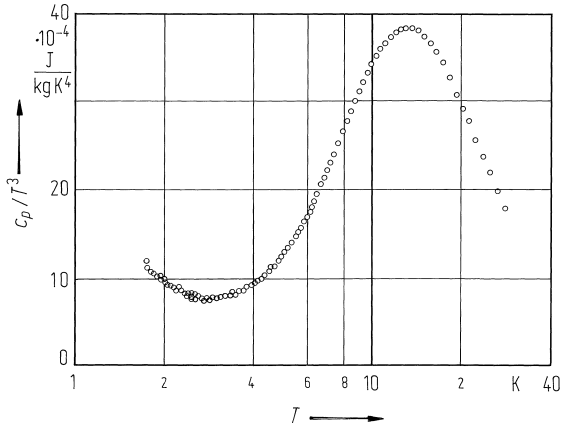

Fig. 1A-15-028. $PbZrO_3$ (ceramics). c_p / T^3 vs. T [84Law].
c_p: specific heat capacity at constant pressure.

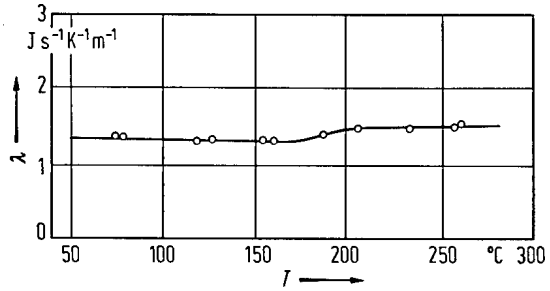

Fig. 1A-15-029. $PbZrO_3$ (ceramics). λ vs. T [60Yos]. λ: thermal conductivity.

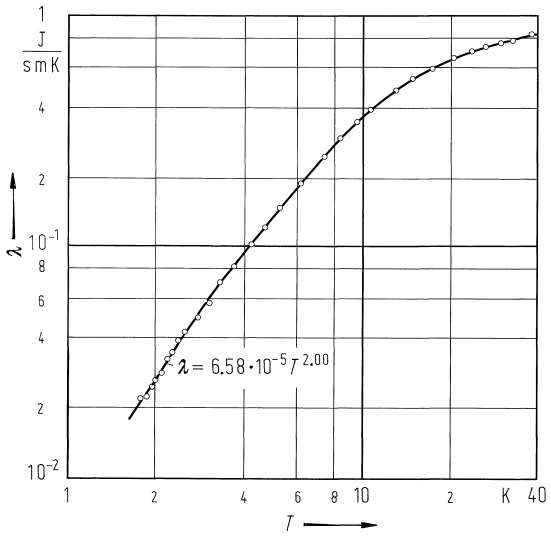

Fig. 1A-15-030. $PbZrO_3$ (ceramics). λ vs. T [84Law]. λ: thermal conductivity.

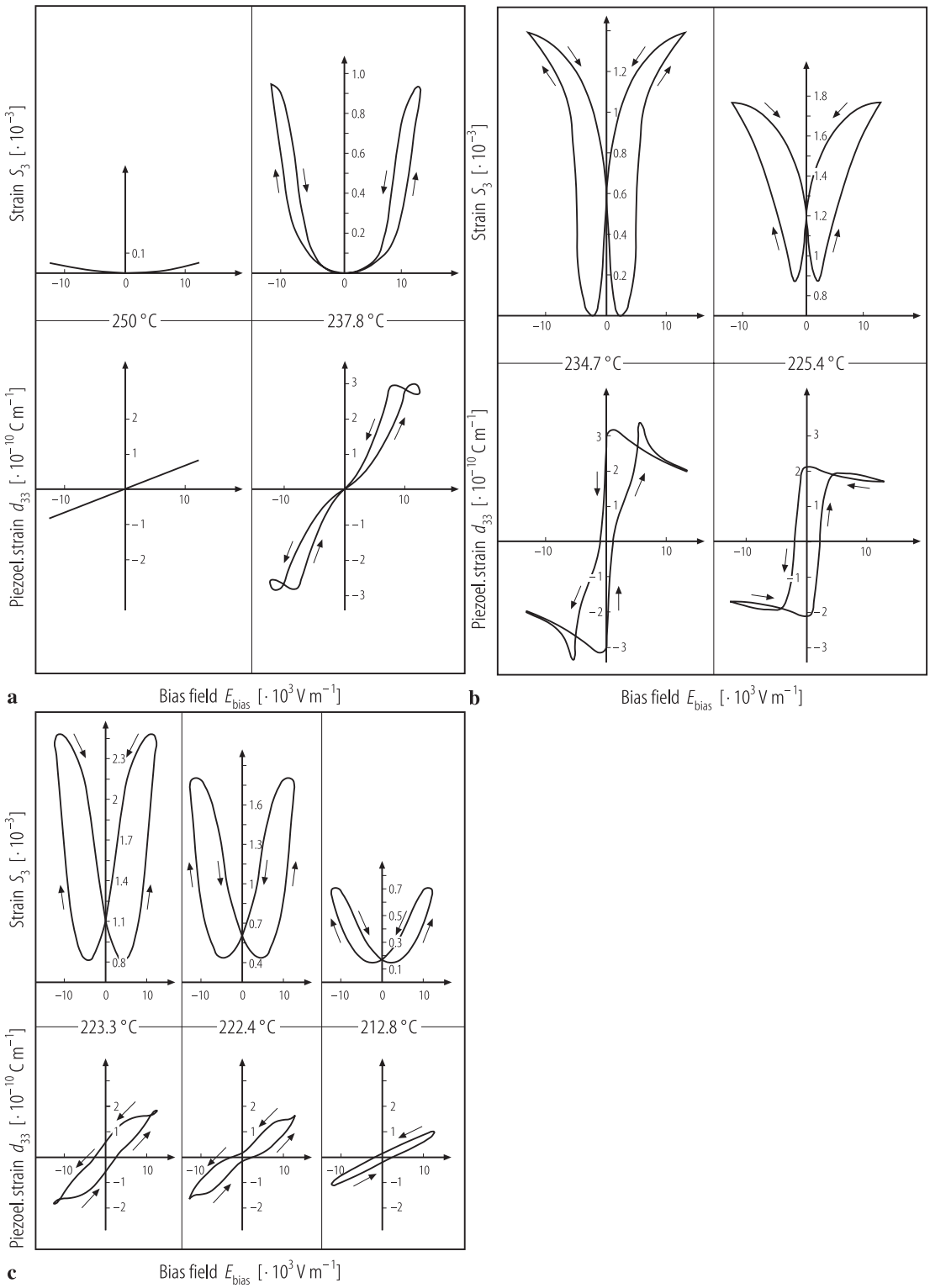

Fig. 1A-15-031. $PbZrO_3$ (ceramics). S_3, d_{33} vs. E_{bias} [89Von]. (**a**): paraelectric phase. (**b**): intermediate phase which appears on cooling. (**c**): antiferroelectric phase.

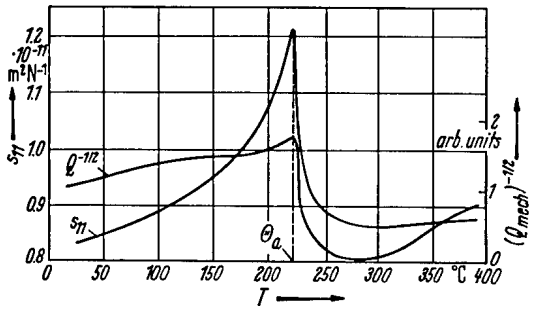

Fig. 1A-15-032. $PbZrO_3$ (ceramics). s_{11}, $(Q_{mech})^{-1/2}$ vs. T [55Mar]. s_{11}: elastic compliance, Q_{mech}: mechanical Q factor, porosity = 0.12.

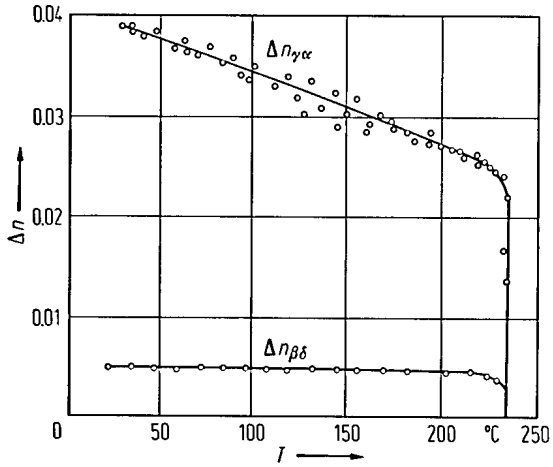

Fig. 1A-15-033. $PbZrO_3$. Δn vs. T [55Jon]. $\Delta n_{\gamma\alpha} = n_b - n_a$, $\Delta n_{\beta\delta} = n_c - n_\delta$. n_a , n_b , n_c , n_δ : refractive indices along orthorhombic [100], [010], [001], [110] directions, respectively. Wavelength: Na light.

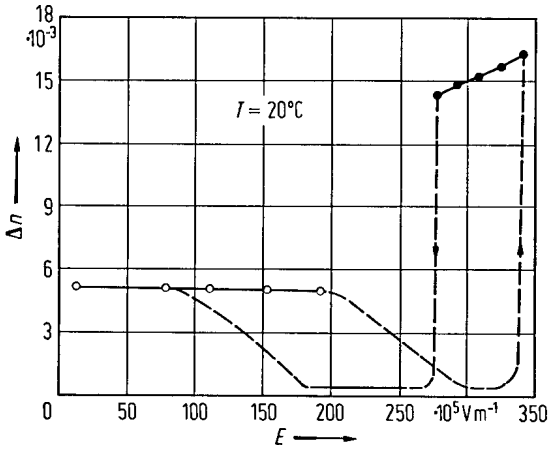

Fig. 1A-15-034. $PbZrO_3$. Δn vs. E [76Fes2]. E was applied along the [210] direction of the orthorhombic cell. Birefringence was measured over the plane perpendicular to the [210] direction.

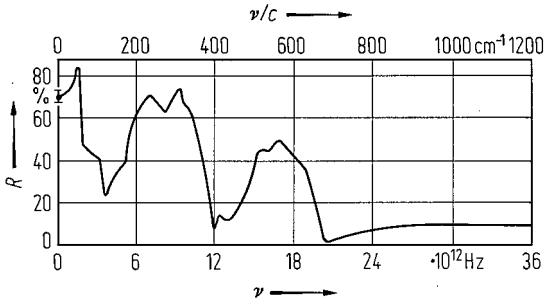

Fig. 1A-15-035. $PbZrO_3$ (ceramics). R vs. ν [65Per]. R: optical reflectance.

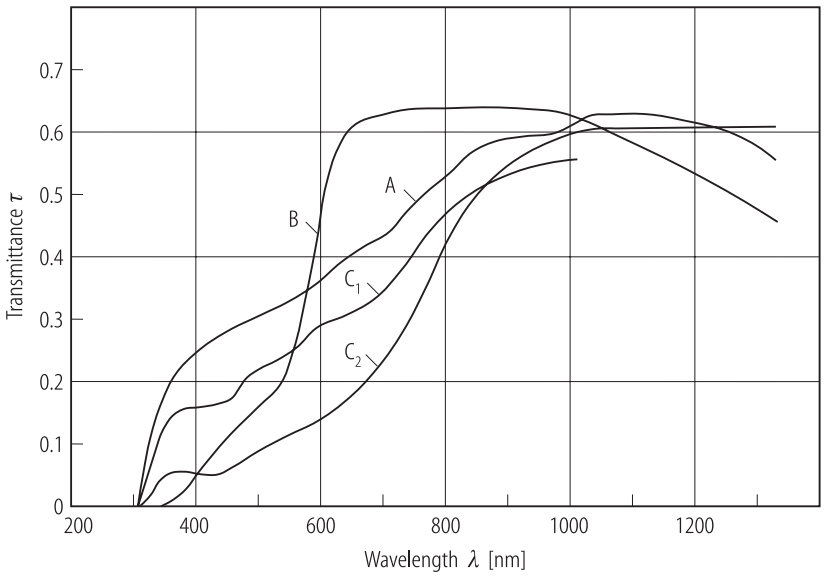

Fig. 1A-15-036. $PbZrO_3$. τ vs. λ at RT [89Woj]. τ: optical transmittance. λ: wavelength. Curve A, B, C: $PbZrO_3$ single crystals grown from solutions with different compositions. Crystal thickness in mm: 0.024, 0.12, 0.037, 0.0813 for A, B, C_1, C_2, respectively.

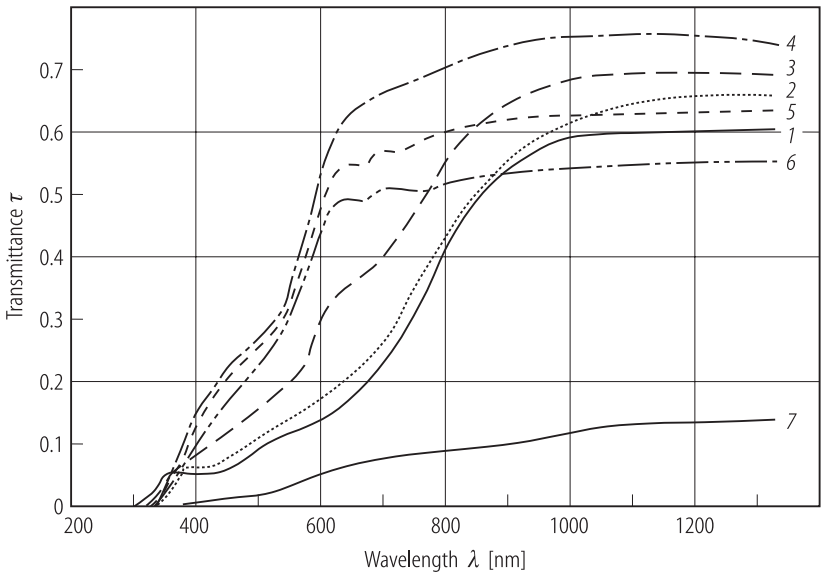

Fig. 1A-15-037. $PbZrO_3$. τ vs. λ at RT [89Woj]. τ: optical transmittance. λ: wavelength. Parameter: temperature at which the crystal was annealed in vacuum (10^3 Pa) for 15 min. Curve *1*: without annealing, *2*: 600 °C, *3*: 700 °C, *4*: 750 °C, *5*: 800 °C, *6*: 900 °C, *7*: 1000 °C.

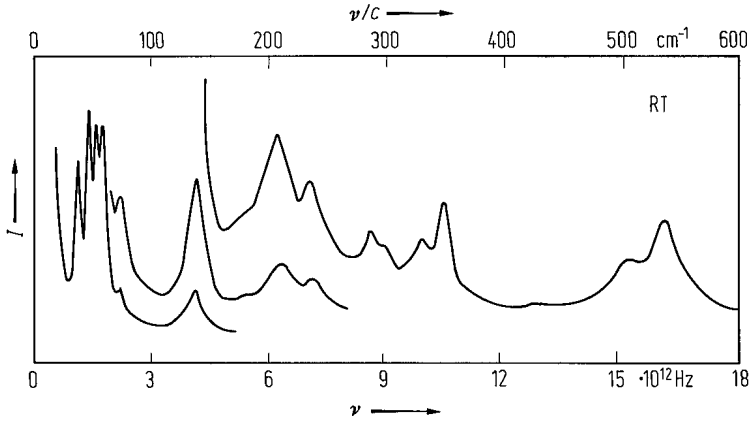

Fig. 1A-15-038. $PbZrO_3$. Raman spectrum [73Pas].

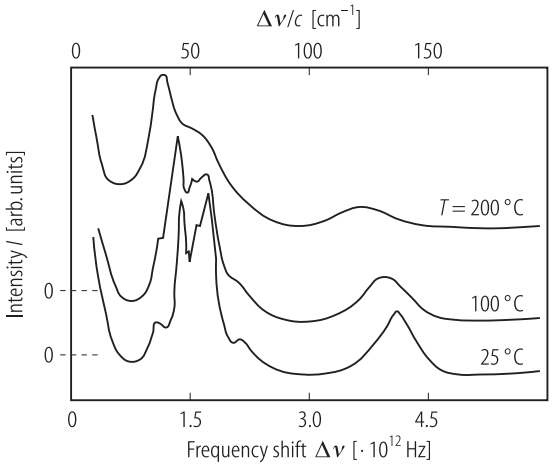

Fig. 1A-15-039. $PbZrO_3$. I vs. $\Delta\nu$ [88Rol]. I: Raman scattering intensity. $\Delta\nu$: frequency shift. Parameter: T.

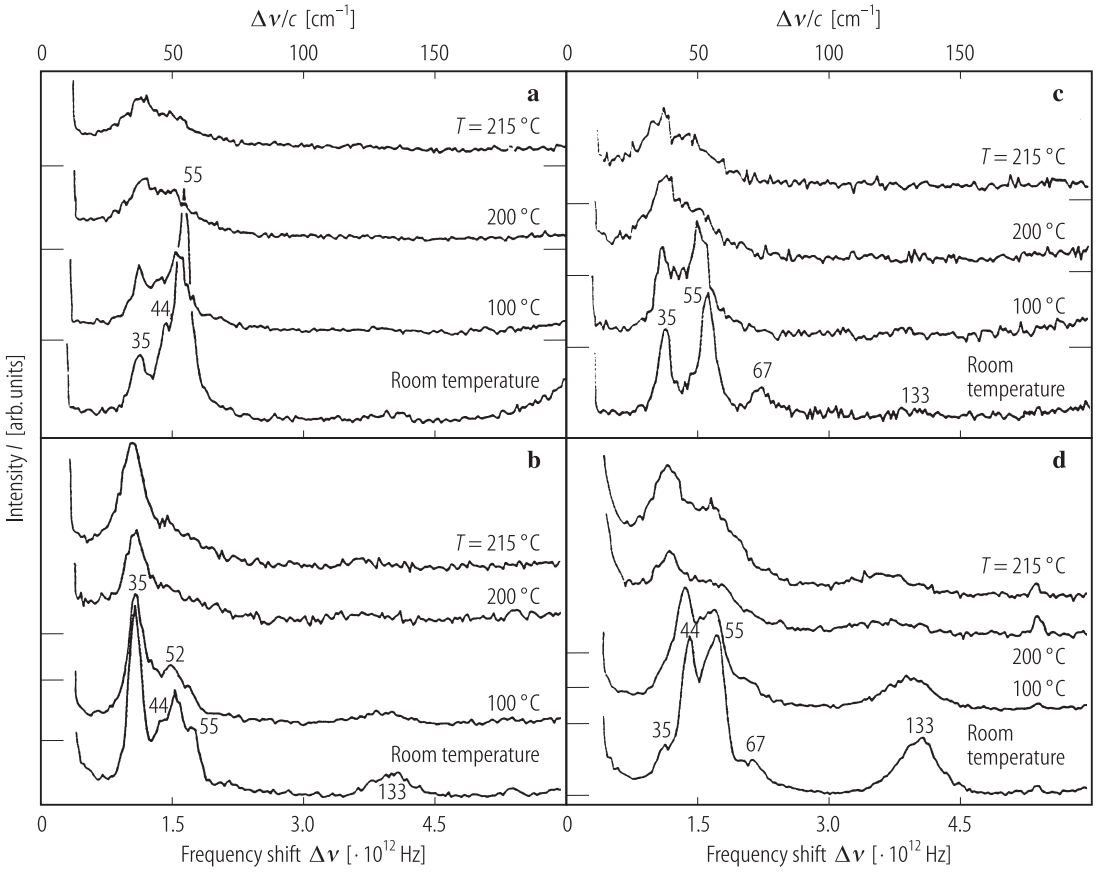

Fig. 1A-15-040. $PbZr_{1-x}Ti_xO_3$ (low Ti content). *I* vs. $\Delta\nu$ [89Rol2]. *I*: Raman scattering intensity. $\Delta\nu$: frequency shift. Parameter: *T*. Scattering geometries: (**a**): *X(ZZ)Y*, (**b**): *X*(*YY*)*Z*, (**c**): *X*(*YX*)*Y*, (**d**): *X*(*ZY*)*Z*.

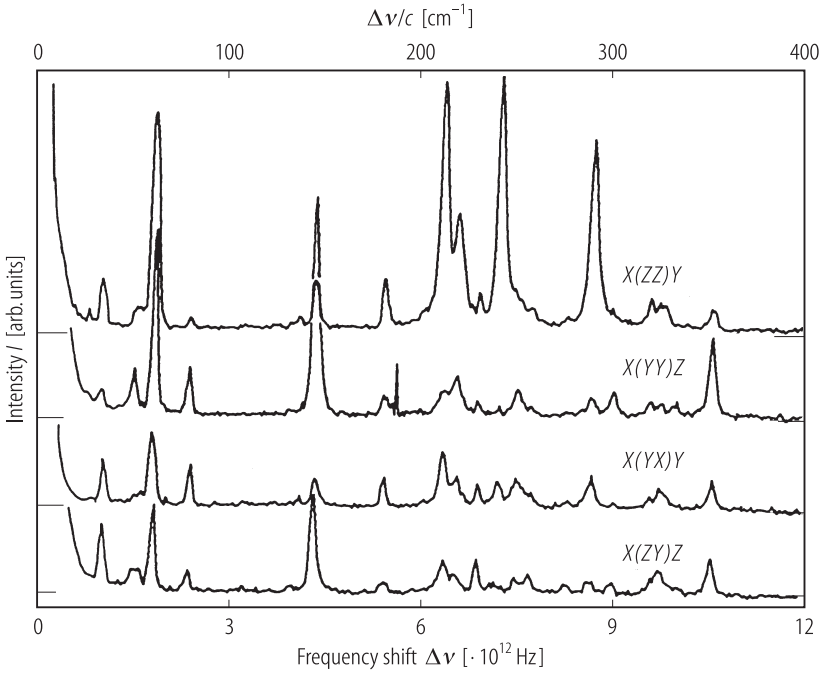

Fig. 1A-15-041. $PbZr_{1-x}Ti_xO_3$ (low Ti content). *I* vs. $\Delta\nu$ [89Rol2]. *I*: Raman scattering intensity at 10 K. $\Delta\nu$: frequency shift. Parameter: scattering geometry.

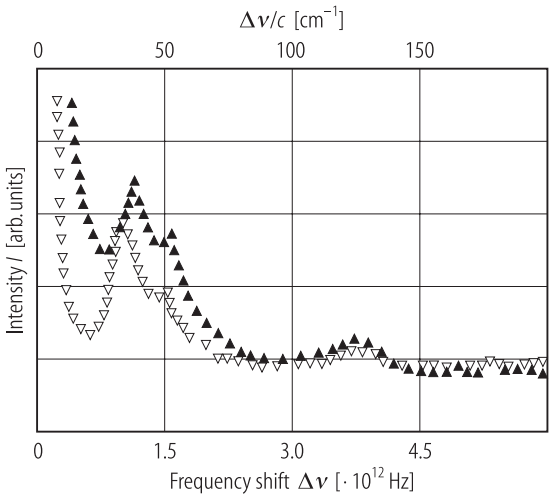

Fig. 1A-15-042. $PbZr_{1-x}Ti_xO_3$ (low Ti content). *I* vs. $\Delta\nu$ [89Rol2]. *I*: Raman scattering intensity at 150 °C. $\Delta\nu$: frequency shift. Parameter: scattering geometry, full triangles: *X*(*ZY*)*Z*, open triangles upside-down: *X*(*YY*)*Z*.

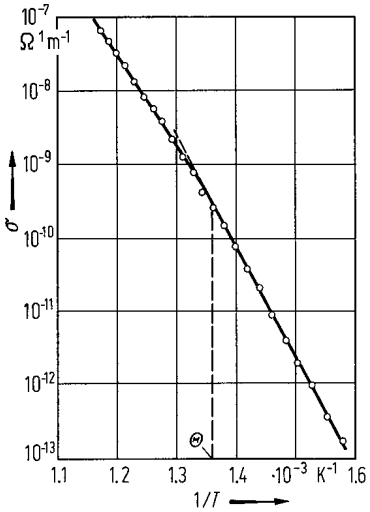

Fig. 1A-15-043. $PbZrO_3$ (ceramics). σ vs. T^{-1} [72Ujm]. σ: electrical conductivity in $\Omega^{-1}cm^{-1}$. Pt–$PbZrO_3$–Pt system. Activation energy: ΔU = 1.31 eV for T < 455 °C, ΔU = 1.03 eV for T > 465 °C.

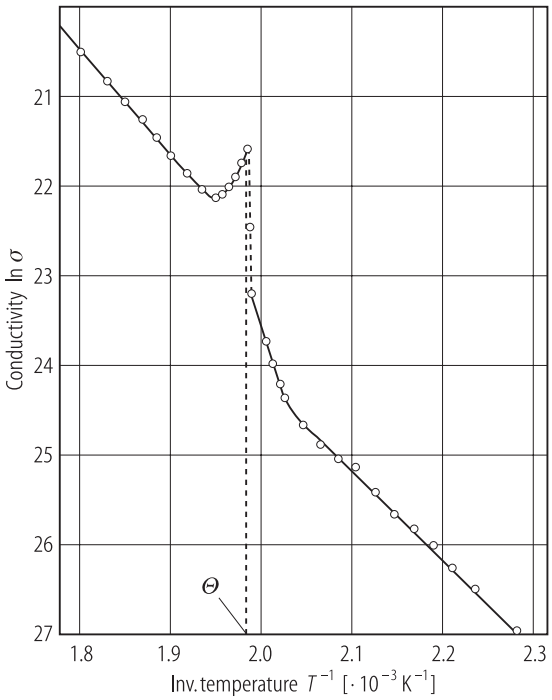

Fig. 1A-15-044. $PbZrO_3$ (single crystal). $\ln\sigma$ vs. T^{-1} [78Ujm]. σ: electrical conductivity in Ω^{-1} cm^{-1}. Ag–$PbZrO_3$–Ag system. The activation energy: ΔU = 1 eV in phase I, ΔU = 0.9 eV in phase II.

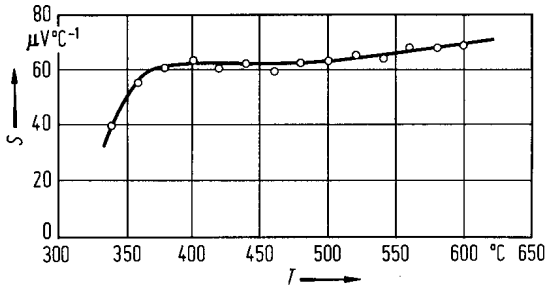

Fig. 1A-15-045. $PbZrO_3$ (ceramics). *S* vs. *T* [72Ujm]. *S*: Seebeck coefficient. Pt–$PbZrO_3$–Pt system. p-type conduction.

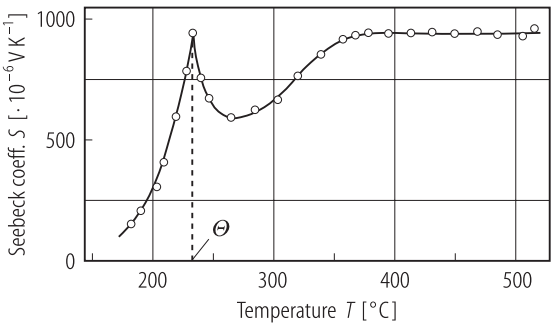

Fig. 1A-15-046. $PbZrO_3$ (ceramics). *S* vs. *T* [75Ujm]. *S*: Seebeck coefficient. Au–$PbZrO_3$–Au system. p-type conduction.

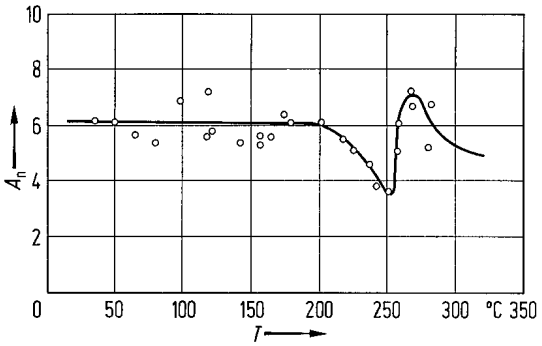

Fig. 1A-15-047. $PbZrO_3$:^{119} * Sn. A_n vs. T [70Jai].
A_n: normalized area of Mössbauer absorption spectra.

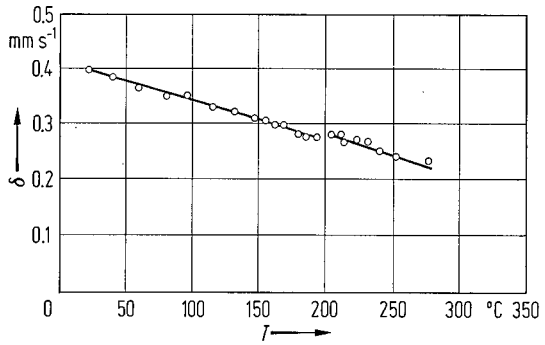

Fig. 1A-15-048. $PbZrO_3$: 5mol% $BiFeO_3$. δ vs. T [71Can].
δ: isomer shift.

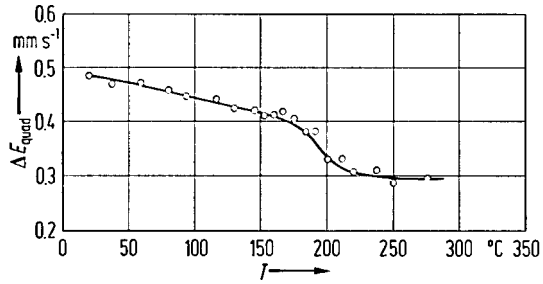

Fig. 1A-15-049. $PbZrO_3$: 5mol% $BiFeO_3$. ΔE_{quad} vs. T [71Can]. ΔE_{quad}: quadrupole splitting in Mössbauer spectrum.

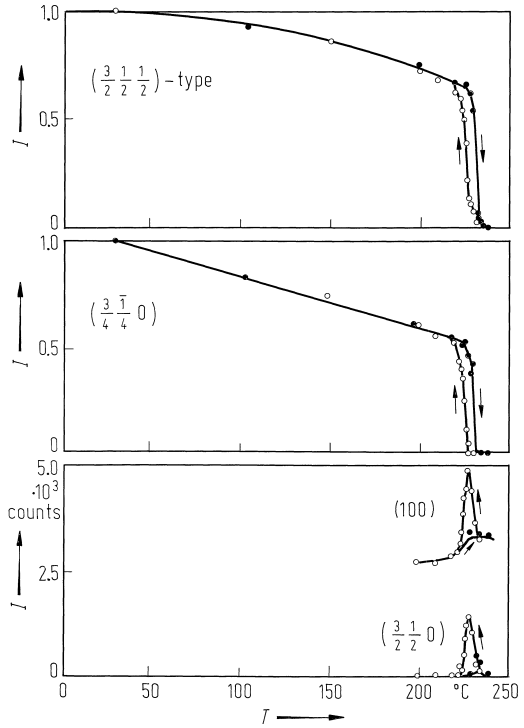

Fig. 1A-15-050. $PbZrO_3$. *I* vs. *T* [84Fuj]. *I*: integrated intensity of superlattice reflection with wave vector $\boldsymbol{q}_\Sigma$, $\boldsymbol{q}_R$ or $\boldsymbol{q}_M$. Full circles: on heating, open circles: on cooling. The intensity of weak reflection (100) is shown for comparison.

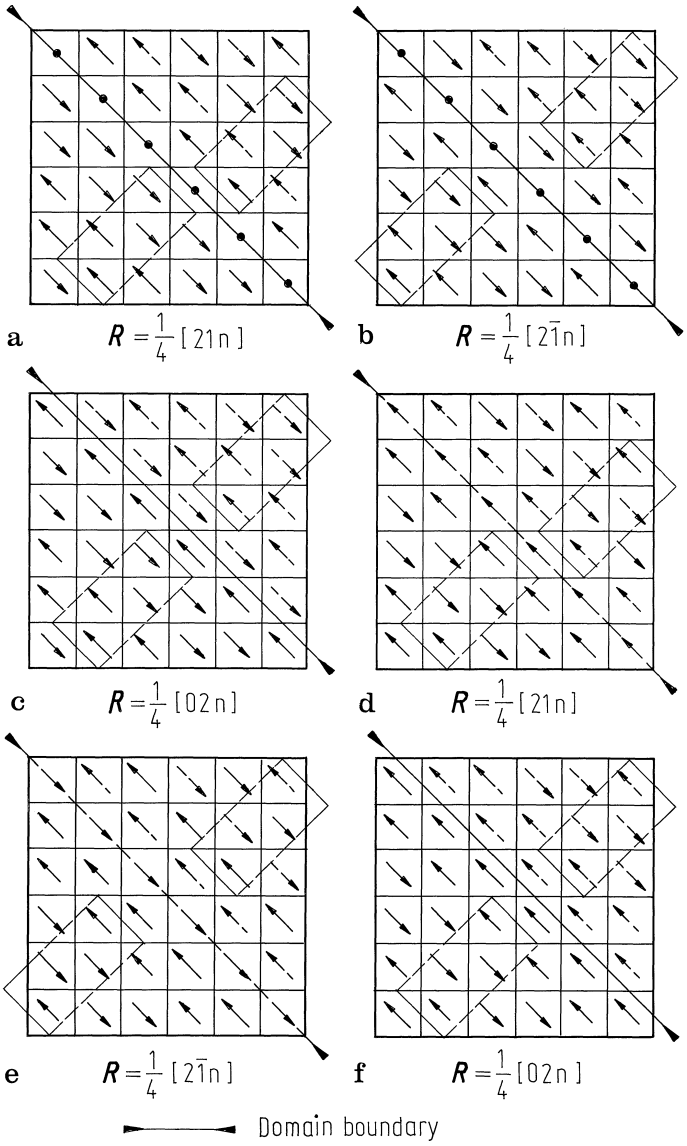

Fig. 1A-15-051. $PbZrO_3$. 180°-domains configuration for three displacement vectors ***R*** [82Tan2]. (**a**), (**d**): ***R*** = (1/4)[21n]; (**b**), (**e**): ***R*** = (1/4)$[2\bar{1}n]$; (**c**), (**f**): ***R*** = (1/4)[02n]. n = 0 or 2.

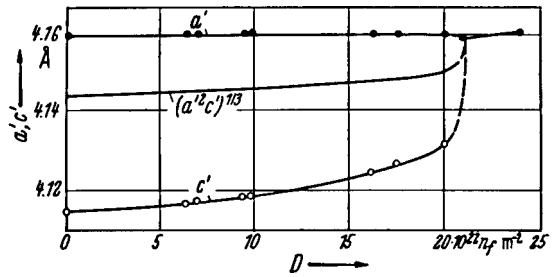

Fig. 1A-15-052. $PbZrO_3$. Lattice parameters a', c', $(a'^2c')^{1/3}$ vs. D [66Hau]. a', c' referred to the pseudotetragonal unit cell. D: dose of fast neutrons (n_f).

References

50Rob Roberts, S.: J. Am. Ceram. Soc. **33** (1950) 63.
50Shi Shirane, G., Sawaguchi, E., Takeda, A.: Phys. Rev. **80** (1950) 485.
50Smo Smolenskii, G.A.: Zh. Tekh. Fiz. **20** (1950) 137.
51Saw1 Sawaguchi, E., Maniwa, H., Hoshino, S.: Phys. Rev. **83** (1951) 1078.
51Saw2 Sawaguchi, E., Shirane, G., Takagi, Y.: J. Phys. Soc. Jpn. **6** (1951) 333.
51Shi Shirane, G., Sawaguchi, E., Takagi, Y.: Phys. Rev. **84** (1951) 476.
51Ued Ueda, R., Shirane, G.: J. Phys. Soc. Jpn. **6** (1951) 209.
52Saw1 Sawaguchi, E.: J. Phys. Soc. Jpn. **7** (1952) 110.
52Saw2 Sawaguchi, E., Kittaka, K.: J. Phys. Soc. Jpn. **7** (1952) 336.
52Shi Shirane, G.: Phys. Rev. **86** (1952) 219.
53Saw Sawaguchi, E.: J. Phys. Soc. Jpn. **8** (1953) 615.
54Shi Shirane, G., Hoshino, S.: Acta Crystallogr. **7** (1954) 203.
55Jon Jona, F., Shirane, G., Pepinsky, R.: Phys. Rev. **97** (1955) 1584.
55Mar Marutake, M., Ikeda, T.: J. Phys. Soc. Jpn. **10** (1955) 424.
57Jon Jona, F., Shirane, G., Mazzi, F., Pepinsky, R.: Phys. Rev. **105** (1957) 849.
60Yos Yoshida, I.: J. Phys. Soc. Jpn. **15** (1960) 2211.
64Fus Fushimi, S., Ikeda, T.: Jpn. J. Appl. Phys. **3** (1964) 171.
65Per Perry, C.H., McCarthy, D.H., Rupprecht, G.: Phys. Rev. **138** (1965) A1537.
65Pet Petrov, V.M.: Izv. Akad Nauk SSSR, Ser. Fiz. **29** (1965) 933; Bull. Acad. Sci. USSR, Phys. Ser. (English Transl.) **29** (1965) 938.
66Hau Hauser, O., Schenk, M.: Phys. Status Solidi **18** (1966) 547.
66Rap Rapoport, E.: Phys. Rev. Lett. **17** (1966) 1097.
67Fus Fushimi, S., Ikeda, T.: J. Am. Ceram. Soc. **50** (1967) 131.
68Kuz Kuznetzov, V.A.: J. Cryst. Growth **3, 4** (1968) 405.
69Gou Goulpeau, L.: Phys. Status Solidi **32** (1969) K1.
69Tsu Tsuzuki, K., Sakata, K., Wada, M.: Jpn. J. Appl. Phys. **8** (1969) 816.
70Jai Jain, A.P., Shringi, S.N., Sharma, M.L.: Phys. Rev. **132** (1970) 2756.
70Sam Samara, C.A.: Phys. Rev. B **1** (1970) 3777.
71Can Canner, J.P., Yagnik, C.M., Cerson, R., James, W.J.: J. Appl. Phys. **42** (1971) 4708.
72Sco Scott, B.A., Burns, G.: J. Am. Ceram. Soc. **55** (1972) 331.
72Ujm Ujma, Z., Olech, J., Wrobel, Z.: Acta Phys. Polon. A **41** (1972) 179.
73Pas Pasto, A.E., Condrate Sr, R.A.: J. Am. Ceram. Soc. **56** (1973) 436.
74Ein Einsiedel, H.V., Rosenblum, S.S.: Phys. Status Solidi (b) **65** (1974) K5.
74Mar Marbeuf, A., Ravez, J., Demazeau, G., Hagenmuller, P.: Bull. Soc. Chim. France, 1974, 1871.
74Sha Shatalova, G.E., Filip'ev, V.S., Katsnel'son, L.M., Fesenko, E.G.: Kristallografiya **19** (1974) 412; Sov. Phys. Crystallogr. (English Transl.) **19** (1974) 257.
74Ujm Ujma, Z.: Acta Phys. Polon. **A45** (1974) 773.
75Sai Saitovitch, H., Fechner, J.B.: Phys. Status Solidi (b) **69** (1975) 595.
75Tei Teisseron, G., Baudry, A.: Phys. Rev. B **11** (1975) 4518.
75Ujm Ujma, Z., Handerek, T.: Phys. Status Solid (a) **28** (1975) 489.
76Fes1 Fesenko, O.E.: Dokl. Akad. Nauk SSSR **229** (1976) 1109; Sov. Phys. Dokl. (English Transl.) **21** (1976) 43l.
76Fes2 Fesenko, O.E., Smotrakov, V.G.: Ferroelectrics **12** (1976) 211.
76Pro Prokopalo, O.I.: Ferroelectrics **14** (1976) 683.
78Fes Fesenko, O.E., Kolesova, R.V., Sindeyev, Yu.G.: Ferroelectrics **20** (1978) 177.
78Han Handerek, J., Wrobel, Z., Wojcik, K., Ujma, Z.: Ferroelectrics **18** (1978) 127.
78Pro Prokopalo, O.I., Fesenko, E.G., Malitskaya, M.A., Popov, Yu.M., Smotrakov, V.U.: Ferroelectrics **18** (1978) 99.

78Ujm Ujma, Z., Handerek, J.: Acta Phys. Polon. **A53** (1978) 665.
79Fes Fesenko, O.E., Kolesova, R.V., Sindeyev, Yu.G.: Fiz. Tverd. Tela **21** (1979) 1152; Sov. Phys. Solid State (English Transl.) **21** (1979) 668.
79Fuj Fujishita, H., Shiozaki, Y., Sawaguchi, E.: J. Phys. Soc. Jpn. **46** (1979) 1391.
80Pri Prisedsky, V.V., Komarov, V.P., Pan'ko, G.F., Klimov, V.V.: Ferroelectrics **23** (1980) 23.
81Ism Ismailzade, I.H., Ismailov, R.M., Alekberov, A.I.: Ferroelectrics **31** (1981) 165.
82Fuj Fujishita, H., Shiozaki, Y., Achiwa, N., Sawaguchi, E.: J. Phys. Soc. Jpn. **51** (1982) 3583.
82Sin Singh, K., Indurkar, A., Deshmukh, K.G.: Ferroelectrics **45** (1982) 219.
82Tan1 Tanaka, M., Saito, R., Tsuzuki, K.: J. Phys. Soc. Jpn. **51** (1982) 2635.
82Tan2 Tanaka, M., Saito, R., Tsuzuki, K.: Jpn. J. Appl. Phys. **21** (1982) 291.
84Fuj Fujishita, H., Hoshino, S.: J. Phys. Soc. Jpn. **53** (1984) 226.
84Law Lawless, W.N.: Phys. Rev. B **30** (1984) 6555.
84Leo Leont'ev, N.G., Kolesova, R.V., Fesenko, O.E., Smotrakov, V.G.: Kristallografiya **29** (1984) 398; Sov. Phys. Crystallogr. (English Transl.) **29** (1984) 240.
84Rol Roleder, K., Wojcik, K.: Ferroelectrics **61** (1984) 293.
84Ujm Ujma, Z.: Phase Transitions **4** (1984) 169.
84Zam Zametin, V.I.: Phys. Status Solidi (b) **124** (1984) 625.
85Ujm Ujma, Z., Handerek, J., Pisarski, M.: Ferroelectrics **64** (1985) 237.
86Rol Roleder, K., Handerek, J., Ujma, Z., Kania, A.: Ferroelectrics **70** (1986) 181.
88Lan Lanagan, M.T., Kim, J.H., Jang, S., Newnham, R.E.: J. Am. Ceram. Soc. **71** (1988) 311.
88Rol Roleder, K., Kugel, G.E., Handerek, J., Fontana, M.D., Carabatos, C., Hafid, M., Kania, A.: Ferroelectrics **80** (1988) 161.
88Ujm Ujma, Z., Dmytrow, D., Handerek, J.: Ferroelectrics **81** (1988) 107.
89LiS Li, S., Condrate, Sr., R.A., Jang, S.D., Spriggs, R.M.: J. Mater. Sci. **24** (1989) 3873.
89Rol1 Roleder, K., Dec, J.: J. Phys. Condens. Matter **1** (1989) 1503.
89Rol2 Roleder, K., Kugel, G.E., Fontana, M.D., Handerek, J., Lahlou, S., Carabatos-Nedelec, C.: J. Phys. Condens. Matter **1** (1989) 2257.
89Von Von Cieminski, J., Roleder, K., Handerek, J.: Ferroelectr. Lett. **10** (1989) 9.
89Woj Wojcik, K., Ujma, Z.: Ferroelectrics **89** (1989) 133.
90Hid Hidaka, T., Oka, K.: Ferroelectrics **108** (1990) 171.
90Kug Kugel, G., Lahlou, S., Handerek, J., Ujma, Z., Wojcik, K., Roleder, K., Fontana, M.D., Carabatos-Nedelec, C.: Ferroelectrics **107** (1990) 103.
90Yam Yamakawa, T., Uchino, K.: Proc. IEEE Int. Symp. Appl. Ferroelectr., 7 th, Urbana-Champaign, IL, June 1990, Krupanidhi, S.B., Kurtz, S.K. (eds.), 1990, p. 610.
92Bal Balyunis, L.E., Bah, I.S., Fesenko, O.E.: Izv. Akad. Nauk SSSR, Ser. Fiz. **56** (1992) 142; Bull. Acad. Sci. USSR, Phys. Ser. (English Transl.) **56** (1992) 1601.
93Bal Balyunis, L.E., Topolov, V.Yu., Bah, I.S., Turik, A.V.: J. Phys. Condens. Matter **5** (1993) 1419.
93Law Lawless, W.N.: Ferroelectr. Lett. **15** (1993) 27.
94Bah Bah, I.S., Balyunis, L.E., Topolov, V.Yu., Fesenko, O.E.: Ferroelectrics **152** (1994) 237.
94Men Meng, J., Zou, G., Cui, Q., Zhu, Z., Du, Z.: Solid State Commun. **91** (1994) 519
95Dai Dai, X.H., Li, J.H., Viehland, D.: Phys. Rev. B **51** (1995) 2651.